DEUTSCHES ELEKTRONEN-SYNCHROTRON DESY

DESY SR-76/16
November 1976

Photoionization Resonance Spectra of CO_2^+ and Threshold Electron-Ion Coincidence Measurements of the Fragmentation of CO_2^+

by

R. Frey, B. Gotchev, O. F. Kalman,
W. B. Peatman, H. Pollak and E. W. Schlag
Institut für Physikalische und Theoretische Chemie
Technische Universität München, Germany

2 HAMBURG 52 · NOTKESTIEG 1

To be sure that your preprints are promptly included in the
HIGH ENERGY PHYSICS INDEX ,
send them to the following address (if possible by air mail) :

DESY
Bibliothek
2 Hamburg 52
Notkestieg 1
Germany

Photoionization Resonance Spectra of CO_2^+ and Threshold Electron-Ion Coincidence Measurements of the Fragmentation of CO_2^+ $

R. Frey, B. Gotchev, O. F. Kalman†,
W. B. Peatman*, H. Pollak and E. W. Schlag
Institut für Physikalische und Theoretische Chemie
Technische Universität München, Germany

Abstract

Photoionization Resonance (PIR) spectroscopy has been used to study the vibrational and spin orbit structure of the $\tilde{X}$, $\tilde{A}$, $\tilde{B}$ and $\tilde{C}$ states of CO_2^+. We have determined directly the Renner-Teller-Spin-Orbit interaction parameters for the $\tilde{X}$ state, the ionization potentials for all four states, the $\tilde{A}$ state spin orbit splitting and the ν_1 frequency for the $\tilde{X}$, $\tilde{A}$ and $\tilde{B}$ states. From coincidence measurements between threshold electrons and the ions produced, it was found that only O^+ + CO is produced at the CO_2^+ ($\tilde{C}$) threshold - i.e. no CO_2^+ was detected. It is further estimated that ca. 30 % of the CO produced is in the v = 0 ground state. Finally, the PIR spectrum of CO_2^+ just below the $\tilde{C}$ state suggests that the bond dissociation energy of CO_2 has an upper limit of about 5.44 eV.

† Present Address: Iowa State University, Ames

* Alfred P. Sloan Research Fellow
Permanent Address: Chemistry Department,
Vanderbilt University, Nashville, Tennessee

$ Work supported by Deutsche Forschungsgemeinschaft DFG and Deutsches Elektronensynchrotron DESY

Introduction

The photoionization of gas phase molecules is a powerful tool for observing states of the ion. Traditionally photoionization studies are performed either by a study of photoion current with wavelength (PI) or secondly by studies of the electrons emitted when the sample is irradiated at fixed wavelength, i.e. photoelectron spectroscopy (PES). The former gives excellent values for molecular ionization potentials, but produces little useful spectral structure at shorter wavelengths, a fact particularly unfortunate in view of the otherwise precisely known energy scale of the optical spectrometer. The theoretical origin of this lack of resolution lies in the problem that each new transition occurs with a stepfunction, and hence adds to all previous transitions, producing a staircase function, whose steps become increasingly ill resolved as the number of overtones and combinations increases. In addition autoionization may cover the structure of direct ionization. If measurements are, however, performed with the additional constraint of detecting only threshold electrons, one again has the possibility of a detection due to δ-funktions when the energy of the level threshold is matched, the Bohr frequency condition. The combination of photoionization, together with efficient threshold detection, again then establishes a conventional spectroscopy with peaks occuring only when new levels are reached, i.e. photoionization currents appear only when resonances of the ion occur. It is essential, for this method, to have an intrinsically accurate and highly efficient means of analyzing and detecting threshold electrons. These problems have been solved previously /1,2,3/ and we are here

interested in applying this spectroscopy to triatomic molecules. In experimental studies of this photoionization resonance spectroscopy /1,2,3/, the observation of photoionization thresholds, vibrational levels and, recently, rotational levels /4,5/ of the corresponding molecular ions have been reported. The difficulties and limitations inherent in Rydberg series extrapolation methods, photoionization mass spectrometry and photoelectron spectroscopy are for the most part eliminated by the threshold electron technique in which the electron detector intrinsically only transmits threshold electrons, and hence a signal only at resonance./1,2/. A resolution of several meV (ca. 3o cm^{-1}) full-width-half-maximum (FWHM) is readily obtained together with a high transmission factor, an almost impossible requirement for electron energy analysers. In addition, since the threshold analyser is a passive device, that is, no voltages are varied during an experiment and the threshold photoionization processes are all detected in identically the same manner, there is no calibration procedure involved for the analyser. Autoionization processes are also strongly reduced, but these appear to play a much less significant role for polyatomic molecules than for diatomic molecules. For the latter the autoionization processes can practically dominate the total ionization picture /6/. By means of the corresponding ion spectrum, it is easily possible to sort out the few remaining subdued peaks in the PIR spectrum which do not correspond to zero energy electrons.

By means of the PIR method, we have studied the $\tilde{X}\ ^2\Pi_g$, $\tilde{A}\ ^2\Pi_u$, $\tilde{B}\ ^2\Sigma_u^+$ and $\tilde{C}\ ^2\Sigma_g^+$ states of CO_2^+. One of the more interesting

aspects of CO_2^+ is the expected Renner-Teller splitting in the $^2\Pi$ states when the ν_2 bending vibration is excited /7/. In addition, there is a considerable spread in the values of the ν_1 frequency for the $\tilde{X}$, $\tilde{A}$, and $\tilde{B}$ states that have been reported in the literature /8,9,10,11,12,13,14,15/. Ionization potentials for these four states are also reported here and are in good agreement with values previously reported. In addition to the spectroscopic parameters for CO_2^+, we have studied the dissociation of CO_2^+ ($\tilde{C}$) by means of detecting the threshold electrons and corresponding ions in coincidence with each other in order to conclusively determine the origin of the ions produced. Previous studies on the dissociation of CO_2^+ /16,17,18/ indicate that the $\tilde{C}$ state of CO_2^+ is highly unstable even though the only energetically allowed exit channel is a spin forbidden transition. Fluorescence measurements from CO_2^+ have also suggested that the $\tilde{C}$ state rapidly undergoes dissociation /19,20/ i.e. no fluorescence from this state has been seen.

Finally, the production of O^+ below the threshold of the CO_2^+ $\tilde{C}$ state is reported here. It has been previously suggested /18/ that dissociating Rydberg states produce O + CO which is then quickly followed by ionization of the O.

Experimental

A schematic drawing of the electron-ion optical system is shown in figure 1. The optical parts were constructed out of molybdenum and the entire electron-ion optical system was housed in a Mu-metal magnetic shield, which yielded a residual field of less than 1 milligauss. The electron optics set-up is an improved version of the steradiency analyser previously described /1,2/ and yields an optimal resolution, FWHM, of 0.003 eV with an accelerating voltage of 2.0 V. The ion optics consist of two accelerating stages, two lens stages and a quadrupole mass spectrometer. The lenses enable one to obtain a suitable narrow flight time dispersion for molecular ions and to focus the ion beam on the entrance of the quadrupole mass analyser. The coincidence system calibration and flight time measurements are described below.

Two light sources were used for these experiments: The He-Hopfield continuum, produced in a modified Hinteregger lamp using a commercial high power pulse generator, was used for all of the preliminary experiments along with a 1 meter, scanning VUV monochromator. Most of the data reported here, on the other hand, were measured using synchrotron radiation from the DORIS storage ring at DESY, in Hamburg, Germany. A three meter, ultrahigh vacuum scanning monochromator was used to disperse the radiation/36/.Although the light coming from such a synchrotron-monochromator combination is extensively polarized, the polarization of the light plays no role in threshold electron experiments such as those made here. For all of the data reported here, a photon resolution of 0,15 Å

was used. The standard sodium salicylate-photomultiplier combination was used to measure the transmitted photon intensity. The sodium salicylate film was renewed during the course of the experiments in order to be certain that its efficiency had not altered. The electrons, ions and photons were measured as pulses using suitable detectors, pulse amplifiers, descriminators and computer controlled electronic counters. At the highest photon intensities, approaching 10^8 photons/sec , a x 100 neutral density filter was mounted between the sodium salicylate window and the photomultiplier. The photon intensity measured using the filter and pulse intensity techniques agreed with the photon intensity measured with no filter and with an electrometer.

For the coincidence measurements, additional electronic equipment was required: a gate-and-delay generator, a time-to-pulse-height converter and a pulse-height-analyser being the main components. In all of the experiments, the raw data (photon, electron, ion, coincident electron-ion pairs and wavelength of the monochromator as provided by a shaft encoder on the monochromator) were transferred to a computer and stored directly on magnetic tape for concurrent and subsequent processing. The threshold electron data and the ion data (below) have been normalized point for point by the computer for incident light intensity.

The vacuum system for the ion-electron optics has a base pressure of about 2×10^{-7} Torr using a turbomolecular pumping system. The spectra were made at sample pressures in the range $1 - 6 \times 10^{-5}$ Torr. High purity sample gases used, Ar, Kr, Xe, O_2 and CO_2, all

at room temperature, were taken directly from lecture bottles. During the normal course of the experiments, mass spectra of each sample were made to check the purity. Two modes of operation were employed for the measurements reported here: For the ion and threshold electron spectra, the optics were operated in a static (non-pulsed) mode. Thus, for the electron scans, a 2 Volt acceleration voltage (0.40 V/cm) was used while for the ions 50 Volts (10 V/cm) were applied. For the coincidence measurements, the photoionization region was pulsed with a 25 Volt rectangular pulse, this pulse being triggered by the arrival of a threshold electron at the electron multiplier. The width and the height of this pulse was varied in the calibration experiments in order to verify that the system behaved as expected.

System Characteristics and Calibration

Electron optics: In figure 2a is shown the threshold electron spectrum of Argon with a FWHM of 0.0044 eV. Extracting the photon bandwidth (0.15 Å), an electron analyser FWHM of approximately 0.003 eV is obtained. The intensity ratio deviates from 2:1 because of the presence of the autoionizing 11s'-state of Ar which lies about .003 eV above the $^2P_{3/2}$ ionization threshold /4/. It is readily seen from figures 2a, 2b that autoionization processes which produce electrons which have more than ca. 0.003 eV are sharply suppressed by the new steradiency analyser and that a new peak directly appears, the $^2P_{1/2}$ state.

The electron analyser voltages and therefore characteristics remain fixed for all of the measurements, both in static and in pulsed operation and for all sample substances. Since the only processes of interest are those which produce threshold electrons, there is no variation in electron transmission for the various measurements.

Ion optics: In contrast to the electron optical system, the transmission of the ion optics must be calibrated against mass and fragmentation energy for these experiments in order to be able to correctly compare the intensities of the fragment measured with that of the parent molecular ion. The mass calibration was made by photoionizing Ar, Kr and Xe and measuring the intensity of each in coincidence with the threshold electrons produced, at the peak of the threshold electron curve. In each of the coincidence measurements, a photon wavelength corresponding to a desired point in the threshold electron spectrum was set and the electrons

and ions measured. The coincidence procedure used was as follows: The electron-ion optical system is set at 2 Volts acceleration suitable for the high resolution threshold electron analysis. When such an electron reaches the electron multiplier, it is amplified, converted to a standard negative logic pulse in a descriminator and then goes both to a delay generator and to a pulse generator. The output of the delay generator goes to the "start" input of a time-to-amplitude converter. The output of the pulse generator, a +25 V pulse of 25 - 100 µsec width goes, in turn, to the electron-ion optical system to draw the ions out of the photoionization region. In the approximately 1,05 µsec between the formation of the electron-ion pair and the application of the 25 V pulse on the optics, the ion moves about 1 mm under the combined influence of the thermal energy of the sample molecules and the 0.4 V/cm accelerating field for the electrons. With 25 V applied, an ion of 40 amu reaches the ion detector and is seen at the "stop" input of the time-to-amplitude converter approximately 52 µsec after the leading edge of the 25 V accelerating pulse. In fact, when the 25 V pulse is applied, the effective electric field just in the ionization region is lower than the nominal field of 5 V/cm because of the field penetration from the electron optics side. The influence of this lower field on the ion flight times was determined by the various tests and taken into account. Various accelerating pulse widths were tried out in order to characterize the behaviour of the system. During the actual experimental runs, a pulse width of 60 µsec was used. For no initial fragmentation energy a coincidence peak FWHM of

about 2 μsec is expected (see calculations below). For the rare gases a value of 1,88 (Ar) to 2,45 (Kr) μsec is experimentally obtained. The experimentally determined variation of ion optical transmission versus mass is given in fig. 3 along with the coincidence measurement of argon which is typical of the rare gas results. Calibrating the ion optics for the effects of initial (fragmentation) energy is somewhat more difficult. Experimentally, one can use the well known process /17/

$$O_2(\tilde{X}^3\Sigma_g^-) + h\nu \longrightarrow O_2^+(\tilde{B}^2\Sigma_g^-, v=0,1) + e^-$$
$$\hookrightarrow O^+(^4S_u) + O(^3P)\,,\ \Delta E_{in} = 1{,}6\ eV(v=0),\ 1{,}74\ eV(v=1)$$

to provide two points in the calibration curve. Fig. 4 shows the flight time distribution for O^+ produced at the threshold of the O_2^+ ($B^2\Sigma_g^-$) v = 0 and v = 1 states, under, of course, the same experimental conditions as for all of the other (rare gas, CO_2) coincidence measurements. As expected from the rejection of trajectories with too large a sidewise velocity component, two peaks are seen in fig. 4. The peak at ca. 30 μsec stems from the forward directed initial velocity vector (from the fragmentation energy) while the peak at 39 μsec stems from the backwards (away from the ion detector) directed velocity vector. The extra "bumps" in the curve result from low counting levels encountered. Nevertheless, the absolute flight times, the spacing of the two peaks and the shape of each of the two peaks all as a function of the two initial energies (v = 0,1) constitute sensitive criteria as to the behaviour of the system. These results were then compared with those obtained by calculating the flight times for the optical system

used here. In the trajectory calculations, the entire actual photoionization region was sampled with a grid of origins and for each origin an isotropic distribution of initial velocity vectors was used folded in with a Maxwellian distribution of thermal velocities. In this way, some 50,000 trajectories were obtained for a given mass and initial energy. From these data, both transmission curves and the time parameters (flight time, peak shape and peak spacing) were obtained. In fig. 3, 4 are shown the flight time distributions for Ar^+ and for O^+ (v = 0,1) respectively, as well as the transmission curve as a function of mass and of initial energy. As seen in these figures the calculated and experimentally observed results agree very closely. By means of the computer program, therefore, one can interpret the flight time distribution for initial energy to an accuracy of approximately 50 meV. For these present data, it was assumed that the parent ion dissociates immediately after formation ($< 10^{-7}$ sec), i.e. it does not travel appreciably before it dissociates.

Spectroscopic Data

Photoionization resonance scans of the threshold electrons produced in the photoionization of CO_2 along with the corresponding CO_2^+ ion scans for the $\tilde{X}$, $\tilde{A}$, $\tilde{B}$, and $\tilde{C}$ states of CO_2^+ are shown in fig. 5, 6, 7 and 8. The transitions observed correspond to the process

(1) $\quad CO_2\ (\tilde{X}\ ^1\Sigma_g^+;\ 0,0,0) + h\nu \longrightarrow CO_2^+(\bar{I},\ v_1,\ v_2,\ v_3) + e^-$

where $\bar{I}$ is the particular electronic state involved ($\tilde{X}$, $\tilde{A}$, $\tilde{B}$ or $\tilde{C}$). That is, the parent molecule is in the ground vibronic state and the only variable is the identity of the upper state.

$\tilde{X}^2\Pi_g$: Fig. 5a, b shows the PIR and ion spectra corresponding to the process given in eq. 1 with $\bar{I} = \tilde{X}^2\Pi_g\ (v_1,\ v_2,\ v_3)$. From the 000 and 100 upper state vibrational levels, we obtain directly the adiabatic ionization potential, the spin-orbit splitting and ν_1 (no anharmonicity considered). The results are shown in tabs. 2 and 3. The peaks lying between 896.3 Å and 893.5 Å correspond to the four $v_2 = 1$ states ($v_1 = v_3 = 0$), $^2\Sigma_u^{(+)}$, $^2\Delta u_{5/2}$ and $^2\Delta u_{3/2}$, $^2\Sigma_u^{(-)}$, arising from the combined effects of spin-orbit and Renner-Teller interactions /7/. Although the four peaks are not well resolved, both the Renner parameter, ϵ, and ω_2 may be obtained. From the data, one can obtain a reasonably good estimate of $\epsilon\omega_2$ from the locations of the two $^2\Sigma$ peaks ($\Delta G = .035$ eV $= 280\ cm^{-1}$) where

$$G = G^+ - G^- = A_{v_2,\ K}^{*} = \left\{ A^2 + (\epsilon\omega_2)^2 \cdot \left[(v_2+1)^2 - K^2 \right] \right\}^{1/2} \qquad (2)$$

Here A is the usual spin-orbit coupling constant determined from the 000 and 100 peak splittings. From eq. 2 and the measured data, a value of $|\epsilon\omega_2| = 113\ cm^{-1}$ is obtained. Because the two inner peaks ($^2\Delta_u$ states) are so undefined, their difference is very uncertain and does not enable one to obtain a reliable value for ϵ or ω_2. However, by using the difference between the 020 band at 892.35 Å, corresponding to the $^2\Pi_{g3/2,\ 1/2}$ states, and the reasonably well defined $^2\Sigma_u^{(+)}$ state of 010 at 896.09 Å, the product $\epsilon\omega_2$ may be separated.

$$\text{Thus, } G^-(v_2, K, \pm\tfrac{1}{2}) = \omega_2(1 - \tfrac{1}{8}\epsilon^2)(v_2+1) - \tfrac{1}{2}A^*_{v_2,K} \pm \frac{\epsilon^2\omega A K(v_2+1)}{8\,A^*_{v_2,K}} \qquad (3)$$

$$= \Delta E_{obs} + G(1,0,\pm\tfrac{1}{2})$$

where $A^*_{v_2,k}$ is given in eq. 2, $E_{obs} = 464\ cm^{-1}$, $A = 159\ cm^{-1}$ and $\epsilon\omega_2 = 113\ cm^{-1}$. The values of ϵ and ω_2, so obtained are shown in table 3.

The location of the combination band at 886.1 Å was not explicitely used in obtaining the above spectroscopic parameters but is in reasonable agreement with the value obtained using ν_1, ν_2 ($= \omega_2$) namely 886.0 Å.

$\tilde{A}\ ^2\Pi_u$: In fig. 6 are shown the PIR and ion spectra corresponding to the $\tilde{A}$ and $\tilde{B}$ states of CO_2^+. Although a Renner effect should be present when the ν_2 bending vibration is excited, we see no clear-cut ν_2 contribution and hence obtain no Renner parameter for this state. The adiabatic ionization potential, spin-orbit constant and ν_1 frequency were directly obtained from the data. No anharmo-

nicity term could be found for ν_1. The several peaks which lie between the well defined ν_1 progression correspond to several of the intense autoionization peaks shown in the ion spectrum. These peaks lie in the wing of the electron analyser transmission curve (fig.2c) and their energy uncertainty is too great to allow for an evaluation of the location of the ion states. The peak at 691.38 Å is, however, unusually strong indicating quite unambiguously that the autoionization process yields electrons with nearly zero energy i.e. that an ion state is also within a few meV of this peak. However, it is at such a high energy, relative to the zero of this $\tilde{A}$-state, that it is difficult to assign uniquely. It is evident also that the ν_1 progression is essentially uninfluenced by autoionization since the intensities of both spin-orbit peaks in each case is essentially the same. The only exception to this is the $v_1 = 1$ pair in which the 3/2 component is clearly intensified.

$B^2\Sigma_u^+$: In fig. 6 are also shown the two transitions seen corresponding to the $\tilde{B}$ state. Clearly the geometry of this state is essentially that of the parent molecule. The ionization potential and ν_1 frequency are given in table 2 and 3.

$C^2\Sigma_g^+$: The PIR spectrum corresponding to the $\tilde{C}$ state of CO_2^+ is shown in fig. 2. Only one peak is clearly seen from which the adiabatic ionization potential for this state is obtained (table 2).

Discussion of the Spectroscopic Parameters

The spectroscopic parameters obtained in the present study are given in tabs. 2 and 3. The adiabatic ionization potentials obtained here agree with those obtained from photoionization mass spectroscopy /18/ photoelectron spectroscopy /8/ and optical spectroscopy /11/. From the behaviour of the photon and electron optical systems with the rare gases, a standard deviation uncertainty of 0.002 eV is estimated for the ionization potentials in this work. From a recent study /15/ of the $\tilde{B}$-$\tilde{X}$ emission spectrum of CO_2^+, the difference in ionization potentials for these states is 4.289 eV which is nearly that reported here (4.291 eV).

The $\tilde{X}$ state spin-orbit coupling constant directly observed here (159 cm^{-1}) agrees well with that obtained from Rydberg series extrapolations /10/ (160 cm^{-1}) and with the value 159.7 cm^{-1} obtained recently from a study of the CO_2^+ $\tilde{B}$-$\tilde{X}$ bands /15/. For the $\tilde{A}\ ^2\Pi_u$ state, a spin-orbit constant of about 90 cm^{-1} has been reported /12/. The value given here 86.4 $\pm$ 5 cm^{-1} should be quite reliable stemming as it does from five pairs of ν_1 vibrations (fig. 6a)

The values of the ν_1 vibrational frequencies for the $\tilde{X}$, $\tilde{A}$ and $\tilde{B}$ states have not been reported in the literature with convincing reproducability /8,15/. For the $\tilde{X}$ state, a value of 1280 cm^{-1} for ν_1 has recently been used for spectrum analysis /15/, this value lying somewhat higher than the value reported here, namely 1250cm^{-1}.

1250 cm^{-1} is also obtained from Rydberg series extrapolations /11/. Photoelectron spectroscopic results yield a still smaller value (1210 cm^{-1} /8/). As also reported in a near threshold electron photoionization experiment /21/, we see no indication of ν_3 excitation in the $\tilde{X}$ state. A discussion of the $\tilde{X}$, ν_2 vibration will be briefly postponed here in order to report first the simpler ν_1 frequencies in the $\tilde{A}$ and $\tilde{B}$ states.

A value of ν_1 = 1131 cm^{-1} for the $\tilde{A}$ state have been reported /10,22/. More recently, from photoelectron spectroscopy /8/ a value of 1100 cm^{-1} was reported. The value we obtain, 1110 cm^{-1} ± 5 cm^{-1}, should be reliable given the amount of data available in our threshold electron spectrum and the apparent lack of interference from autoionizing processes.

For the $\tilde{B}$ state we report a value of 1280 ± 15 cm^{-1} the uncertainty being estimated. This value is in good agreement with the results of optical spectroscopy (1275 cm^{-1} /12/) and photoelectron spectroscopy (1274 cm^{-1} /9/ , 1270 /8/.).

Perhaps the most interesting aspect of the present spectra is the fact that the Renner-Teller-spin-orbit interaction in the $X^2\Pi_g$ state is so apparent. Both $\epsilon\omega_2$ (113 cm^{-1}) and ω_2 (508 cm^{-1}) obtained from our measurements are in excellent agreement with those values reported recently from emission spectra in CO_2^+ /15/, viz. $\epsilon\omega_2$ = 108.0 cm^{-1} and ω_2 = 498 cm^{-1}. The Renner parameters, ϵ, consequently, compare equally well, 0.222 (present work) and 0.217 /15/. One final comment regarding the v_2 = 1 peaks: According to

selection rules for the excitation of ν_2 in linear polyatomic molecules /24/ it should not be possible to excite the v_2 = 1 state from the ground state of CO_2. The fact that it appears in this spectrum indicates that (1) the selection rule is not strong in this photoionization process due to the vibronic interaction or (2) that so called degenerate autoionization processes in which autoionizing states yield electrons of essentially zero kinetic energy /4/, enable these transitions to be seen despite a small or zero direct photoionization cross section. The latter argument is supported by suggestions in the literature /18, 23/ that in this energy region a bent superexcited state of CO_2 exists which dominate the absorption spectrum and the photoionization efficiency curve of CO_2^+ producing irregularly spaced peaks. In addition from the relative intensities of the four v_2 = 1 peaks and the v_2 = 2 peak, it appears quite likely that they are at least in part intensified by autoionization processes. The absence of other autoionization structure in the vicinity of the $\tilde{X}$ state indicates the effectivness of the threshold electron analyser in eliminating energetic electrons and supports the argument (see above) that the energies of such intensified peaks correspond very closely to the energies of the direct photoionization transitions.

The assumption of a bent geometry for the $\tilde{X}$ ion state, which would allow the excitation of the v_2 = 1 state in a simple manner, can be excluded. Recent calculations too give no hint for a bent structure /32/. A spectrum of $\tilde{X}$ (CO_2^+) with high resolution by normal photoelectron spectroscopy /33/, produced with the 736/744 Å Ne I resonance radiation shows a smaller peak in the region of the

$^2\Sigma^+_u$, $^2\Delta_{5/2}$ (010) components. This could suggest, that both explanations for the excitation of $v_2 = 1$ levels should be applied.

In fact, the $v_2 = 2$ peak at 892,4 Å contains two or three Renner-Teller components $^2\Pi_g$ ($^2\phi_g$). The remaining $v_2 = 2$ components should match the $v_1 = 1$, $^2\Pi_{3/2}$ level, resulting in a mixing by the Fermi resonance effect /15/. This is indicated in the broadening of the corresponding peak in the spectrum.

With regard to the coupling of the $\tilde{B}$ (000) state with higher vibrational excited states of the $\tilde{A}$ state, observed as irregularities in the rotational structure of $\tilde{B} - \tilde{X}$ transitions in fluorescence measurements /34/, we find no shift of the $\tilde{A}$ (500) state neighbouring the $\tilde{B}$ (000) state which probably comes from the large separation of these two states. However, in our spectrum only the pure ν_1 vibrational progression in the $\tilde{A}$ state is excited, and no combination of vibrational modes.

Dissociation Processes

From these and previous studies /17,18/ it appears clear that the $\tilde{C}^2\Sigma^+_g$ state of CO_2^+ dissociates rapidly and completely to $O^+(^4S_u)$ + $CO(^1\Sigma^+)$, rapid because no fluorescence has been observed from this state /19,20/. As in the study by Eland /17/ in which the helium 584 Å line was used to ionize the CO_2, we can detect no CO_2^+ at photon energies corresponding to the threshold of the $\tilde{C}$ state. Despite this fact, it is clear from the sharp increase in O^+ intensity at this wavelength (639.53 Å, see fig. 8b) which corresponds exactly to the wavelength of the threshold electron peak (fig. 7), that the O^+ production stems from CO_2^+ ($\tilde{C}$). Since the products of this process correspond by the Wigner-Witmer correlation rules to the dissociation limit of a $^4\Sigma^-_g$ state of CO_2^+ /25/ whereas they result from dissociation of the $^2\Sigma^+_g$ state, the observed process is spin-forbidden. Such spin-forbidden dissociation processes have been observed in other systems as well as in CO_2^+ /26,27,28,29/ and suggest that state mixing in polyatomic molecules is likely and significant and that the spin criterion for determining whether a process is likely or not is not particularly useful at least here /30/. In the case at hand, viz. CO_2^+ ($\tilde{C}$), the fluorescence studies /19,20/ set an upper limit to the lifetime of the $\tilde{C}$ state of ca. 10^{-8} sec. For N_2O^+ where spin-forbidden dissociation has also been observed, the observed lifetime of N_2O^+ ($A^2\Sigma^+$) against predissociation is reported to be 410 ± 90 nsec /29/. Thus, for CO_2^+, the rate of dissociation is more strongly affected by the necessary state mixing than for N_2O^+.

In the coincidence measurements made here between the zero energy electrons at 639.40 Å (fig. 7) and either CO_2^+ ions (fig. 8a), CO^+ ions or O^+ ions (fig. 8b), no trace of true coincidences can be seen in the first or second cases while a well defined peak, corresponding to an O^+ flight time of 32.6 μsec is seen for the third. This is shown in fig. 9. From the calculated flight time spectra, in which an initial dissociation energy of 0.324 eV (CO, v = 0) or 0.058 eV (CO, v = 1) have been included, it is estimated that from an eighth to a third of the CO produced lies in the v = 0 state. This is in good agreement with the coincidence results of Eland which indicated that about 15 % of the CO produced was in the ground vibrational state /17/.

McCulloh /18/ reports peaks in the O^+ photoionization curve between 19.071 eV and 19.39 eV, these being the thresholds for the production O^+ (^4S_u) + CO ($^1\Sigma^+$) (v = 0) and CO_2^+ ($\tilde{C}$, $^2\Sigma^+$, 000). He found that these peaks correlate well with members of Rydberg series converging to the $\tilde{C}^2\Sigma_g^+$ state of CO_2^+ and concluded that Rydberg states predissociate to O + CO ($\tilde{X}^1\Sigma^+$) with subsequent rapid ionization of the O to O^+ below the CO_2^+ ($\tilde{C}$) threshold (fig. 8b) starting also at about 649.9 Å and with essentially the same structure between 650 Å and 640 Å, the main onset of O^+ production. No threshold electron peaks are seen in this region indicating that the dissociating Rydberg states are not within 0.02 eV of the resulting state of O^+ (^4S) + CO($^1\Sigma^+$).This suggests that the minimum energy for the formation of O^+ (^4S) + CO ($\tilde{X}^1\Sigma^+$, v = 0) is 19.078 eV (649.9 Å) - 0.02 eV = 19.06 eV, which in turn yield the bond dissociation energy D_0 (O - CO) = 5.44 eV (using the ionization

potential of atomic oxygen I(O) = 13.618 eV /31/). It appears that the value obtained from thermochemical data: D_0 (O - CO) = 5.453 ± 0.002 eV /18/, is slightly too high.

Conclusions

The spectroscopic data presented here for the $\tilde{X}$, $\tilde{A}$, $\tilde{B}$ and $\tilde{C}$ states of CO_2^+, including the Renner parameter and ν_2 for the $\tilde{X}$ state help to clear up some of the uncertainties that exist regarding these states, especially the ν_1 frequencies. Hence,this is due to PIR-spectroscopy beiing a method, which allows the detection of thresholds for the ionization processes with high resolution, but needs no apparative calibration of the analyser. From PIR spectra one can directly obtain essentially all of the molecular parameters pertaining to each ionic state excited from spectra that are unambiguous and straight forward to interpret.

The coincidence measurements show conclusively that all CO_2^+ ($\tilde{C}^2\Sigma_g^+$) produced at threshold rapidly dissociates to O^+ + CO ($\tilde{X}^1\Sigma^+$). It is estimated that about 30 % of the CO produced is in the v = 0 state. Finally the absence of a threshold electron peak at 650 Å suggests that the O - CO bond dissociation energy has an upper limit of 5.44 eV.

Acknowledgements

Financial assistance for this research from the Deutsche Forschungsgemeinschaft and the Deutsches Elektronensynchrotron (DESY) are greatly appreciated. Drs. C. Kunz, E. E. Koch and especially V. Saile are to be thanked for their help and co-operation during the DESY phase of this work. One of us (W. B. P.) greatfully acknowledges financial support from the Alexander von Humboldt Stiftung.

References

1. W.B. Peatman, T.B. Borne and E.W. Schlag, Chem. Phys. Lett. 3, 492 (1969)

2. T. Baer, W.B. Peatman and E.W. Schlag, Chem. Phys. Lett. 4, 243 (1969)

3. R. Spohr, P.M. Guyon, W.A. Chupka and J. Berkowitz, Rev. Sci. Instrum. 42, 1872 (1971)

4. W.B. Peatman, G.B. Kasting and D.J. Wilson, J. Elec. Spectrosc. 7, 233 (1975)

5. a) W.B. Peatman, Chem. Phys. Lett. 36, 495 (1975)
   b) W.B. Peatman, J. Chem. Phys. 64, 4093 (1976)
   c) W.B. Peatman, J. Chem. Phys. 64, 4368 (1976)

6. P.M. Dehmer and W.A. Chupka, J. Chem. Phys. 62, 4525 (1975)

7. G. Herzberg, Electronic Spectra of Polyatomic Molecules, (Van Nostrand, Princeton, 1966) pp. 34-37

8. D.W. Turner, C. Baker, A.D. Baker and C.R. Brundle, Molecular Photoelectron Spectroscopy, (Wiley-Interscience, London, 1970)

9. J.H.D. Eland and C.J. Danby, Int. J. Mass Spectrom. Ion Phys. 1, 111 (1968)

10. a) S. Mrozowski, Phys. Rev. 60, 730 (1941)
b) ibid. 72, 682 (1947)
c) ibid. 72, 691 (1947)

11. a) Y. Tanaka, A.S. Jursa and F.J. LeBlanc,
J. Chem. Phys. 32, 1199 (1960)
b) ibid. 32, 1205 (1960)

12. Y. Tanaka and M. Ogawa,
Can. J. Phys. 40, 879 (1962)

13. G. Herzberg,
op. cit. p. 594, 597

14. F. Bueso-Sanllehi,
Phys. Rev. 60, 556 (1941)

15. D. Gauyacq, M. Horani, S. Leach and J. Rostas,
Can. J. Phys. 53, 2040 (1975)

16. V.H. Dibeler and J.A. Walker,
J. Opt. Soc. Am. 57, 1007 (1967)

17. J.H.D. Eland,
Int. J. Mass Spectrom. Ion Phys. 9, 397 (1972)

18. K.E. McCulloh,
J. Chem. Phys. 59, 4250 (1973)

19. T.S. Wauchop and H.P. Broida,
J. Geophys. Res. 76, 21 (1971)

20. L.C. Lee and D.L. Judge,
J. Chem. Phys. 57, 4443 (1972)

21. D. Villarejo, R. Stockbauer and M.G. Inghram,
J. Chem. Phys. 48, 3342 (1968)

22. a) J.W.C. Johns, Can. J. Phys. 39, 1738 (1961)
b) ibid. 42, 1004 (1964)

23. M. Krauss, S.R. Mielczarek, D. Neumann and C.E. Kuyatt,
J. Geophys. Res. 76, 3733 (1971)

24. G. Herzberg,
op. cit. pp. 158 - 159

25. G. Herzberg,
op. cit. pp. 281-287

26. J. Troe and H.Gg. Wagner,
Ber. Bunsenges. Physik. Chem. 71, 937 (1967)

27. J.C. Lorquet and C. Cadet,
Int. J. Mass Spectrom. Ion Phys. 7, 245 (1971)

28. B. Brehm, J.H.D. Eland, R. Frey and A. Küstler,
Int. J. Mass Spectrom. Ion Phys. 12, 213 (1973)

29. J.H.D. Eland,
Int. J. Mass Spectrom. Ion Phys. 12, 389 (1973)

30. G. Herzberg,
op. cit. pp. 486-487

31. C.E. Moore,
Natl. Bur. Stand. Ref. Data Ser. 34 (1970)

32. a) L. Cederbaum, W. Dohmke,
private communication
b) W.B. England, B. J. Rosenberg, P.J. Fortune
and A. C. Wahl,
J. Chem. Phys. 65, 684 (1976)

33. F. Breyer, H. Hotop,
private communication

34. S. Leach,
Molec. Energy Transfer
(R. Levine and J. Jortner, ed.)
(Wiley and Sons, New York, Toronto, 1976) pp. 163

35. V. A. Koryoshkin,
Dokl. Akad. Nauk. SSSR, 167, 1035 (1966)

36. V. Saile, M. Skibowski, W. Steinmann, P. Gürtler, E.E. Koch,
and A. Kozevnikov,
Applied Optics, in press

TABLE 1

CO_2 : Threshold Electron Peaks

	Line Nr.	λ (Å)	Peak Height (a.u,)	Designation
$\tilde{X}\ (^2\Pi_g)$	1	899,95	32.31	000 $^2\Pi_{3/2}$
	2	898,66	30.92	000 $^2\Pi_{1/2}$
	3	896,16	7.94	010 $^2\Sigma_u^+$
	4	894,6	3.76	010 $^2\Delta_{u\ 3/2}$
	5	894,1	3.32	010 $^2\Sigma_u^-$
	6	892,43	4.03	020 $^2\Pi_{3/2}$, $^2\Pi_{1/2}$
	7	890,00	7.05	100 $^2\Pi_{3/2}$
	8	888,75	8.07	100 $^2\Pi_{1/2}$
	9	886,23	2.94	110
$\tilde{A}\ (^2\Pi_u)$	1	716,24	1.26	000
	2	715,76	0,96	000
	3	710,52	4.99	100
	4	710,08	3.37	100
	5	707,24	0.63	6_0s
	6	704,96	2.47	200
	7	704,56	2.26	200
	8	700,75	1.37	7_0s
	9	699,48	2.17	300
	10	699,06	1.82	300
	11	696,86	1.09	8_0s
	12	694,3	1.23	400, 9_0s
	13	693,68	1.32	400
	14	691,40	2.99	11_0s
	15	689,92	0.84	12_0d
	16	689,0	0.84	500
	17	688,40	0.89	500
$\tilde{B}\ (^2\Sigma_u^+)$	1	686,20	14.07	000
	2	680,20	0.94	100
$\tilde{C}\ (^2\Sigma_g^+)$	1	639,56	0.84	000

Table 3

Vibrational frequencies (cm^{-1})

	Present work		Optical Spectr.		Fluorescence Spectr.		PES
	ν_1	ν_2	ν_1	ν_2	ν_1	ν_2	ν_1
$\tilde{X}\,^2\Pi_g$	1250±10	508±10	1250[a], 1280[b]	531[e]	1280[f]	498[f]	1210[g]
$\tilde{A}\,^2\Pi_u$	1110± 5	-	1131[b,c]	560[c]	-	-	1100[g]
$\tilde{B}\,^2\Sigma_u$	1280±15	-	1275[d]	-	-	558[f]	1270[g], 1274[h]
$\tilde{C}\,^2\Sigma_g$	-	-	-	-	-	-	1390[g]

Spin-Orbit-Coupling-Constant (cm^{-1})

$\tilde{X}\,^2\Pi_g$	159.±3	160[c]	159.7[f]
$\tilde{A}\,^2\Pi_u$	86.4± 5	90[d]	-

Renner-Parameter

$\tilde{X}\,^2\Pi_g$	0.222±0.014	-	0.217[f]

a: see ref. 11; b: see ref. 22; c: see ref. 10
d: see ref. 12; e: see ref. 35; f: see ref. 15
g: see ref. 8; h: see ref. 9;

Table 2

Adiabatic IP (eV)

	Present work	PI Mass Spectr.[a]	PES[b]	Optical Spectroscopy[c]
$X\,^2\Pi_g$	13,777±0.002	13,773 ± 0.002	13,78(8)	13,769±0.03
$\tilde{A}\,^2\Pi_u$	17,311 ± 0.002	-	17,32(3)	17,312
$\tilde{B}\,^2\Sigma_u$	18,068 ± 0.002	18,076	18,08(2)	18,076
$\tilde{C}\,^2\Sigma_g$	19,386 ± 0.002	19,39	19,40(0)	19,38

a: see ref. 18
b: see ref. 8
c: see ref. 11, 12

Figure Captions

Figure 1: Electron-Ion Optical System

Figure 2: a) Ar PIR-spectrum

b) Ar^+ -ion spectrum

c) Electron analyser transmission curve

Figure 3: a) Transmission curve for the ion-optical system as a function of ion mass.

b) Flight time distribution for Ar^+

Dotted line: observed

Solid line: calculated.

Figure 4: Flight time distributions for a fragmentation process with initial energy:

$$O_2\ (\tilde{X}^3\Sigma_g^+) + h\nu \rightarrow O_2\ (\tilde{B}^2\Sigma_g^+,\ v = 0,1) + e^-$$

$$\downarrow$$

$$O^+ + O \quad \begin{matrix} a) & E = 1{,}6\ eV \\ b) & E = 1{,}7\ eV \end{matrix}$$

Dotted lines: observed

Solid lines: calculated

Figure 5: a) CO_2 PIR spectrum of the $\tilde{X}$ state. The vertical lines designate the vibrational structure including Renner-Teller and spin-orbit splitting.

b) Corresponding ion spectrum

Figure 6: a) CO_2 PIR spectrum of the $\tilde{A}$ and $\tilde{B}$ state.

b) Corresponding ion spectrum

Figure 7: CO_2 PIR spectrum of the $\tilde{C}$ state.

Figure 8: a) CO_2^+-ion spectrum

b) O^+-ion spectrum of the CO_2^+-fragmentation.

Figure 9: Flight time distribution of O^+ from the process:

$$CO_2\ (\tilde{X}^1\Sigma_g^+) + h\nu \rightarrow CO_2^+\ (\tilde{C}^2\Sigma_g^+) + e^-$$

$$\downarrow$$

$$CO\ \begin{pmatrix} v = 0 \\ v = 1 \end{pmatrix} + O^+$$

Dotted line: observed

Solid line: calculated

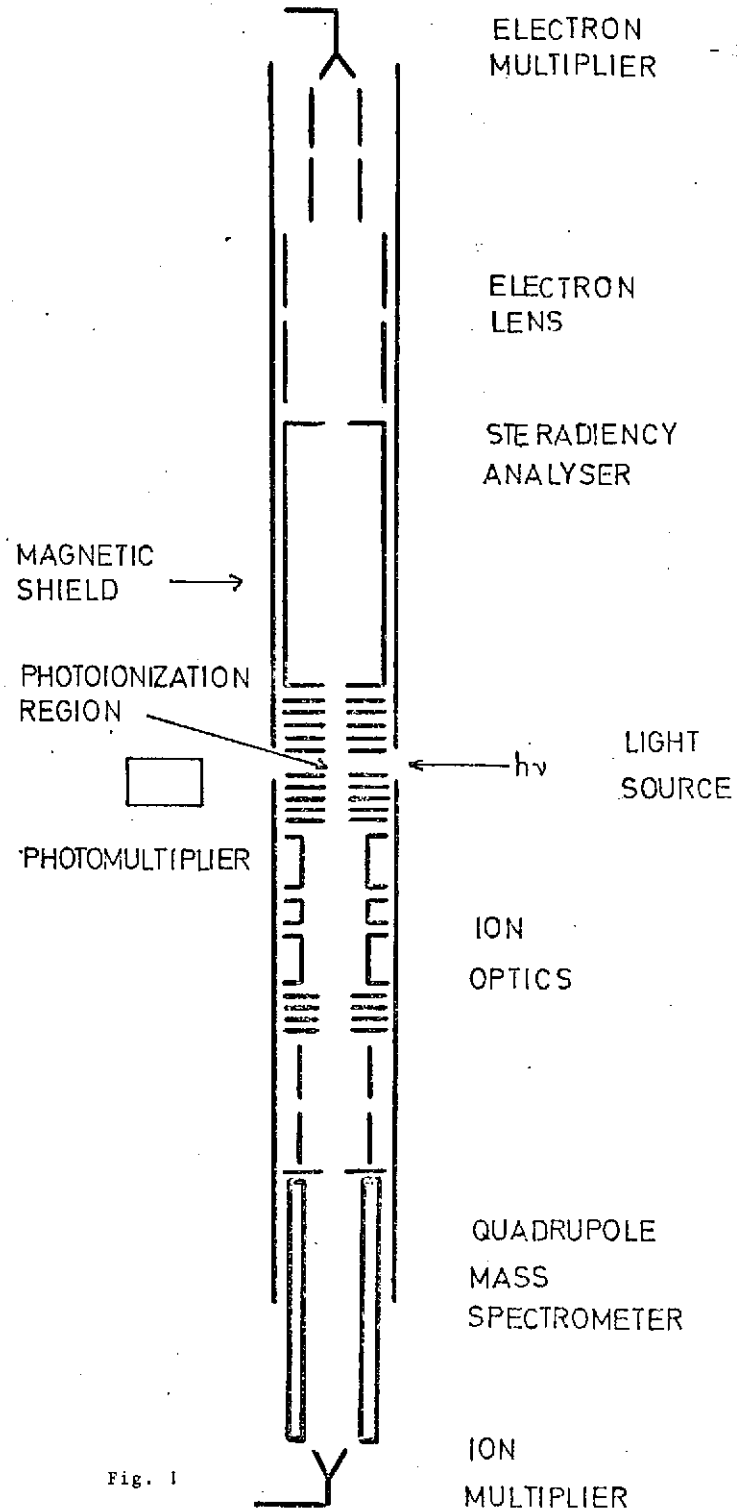

Fig. 1

Fig. 2b)

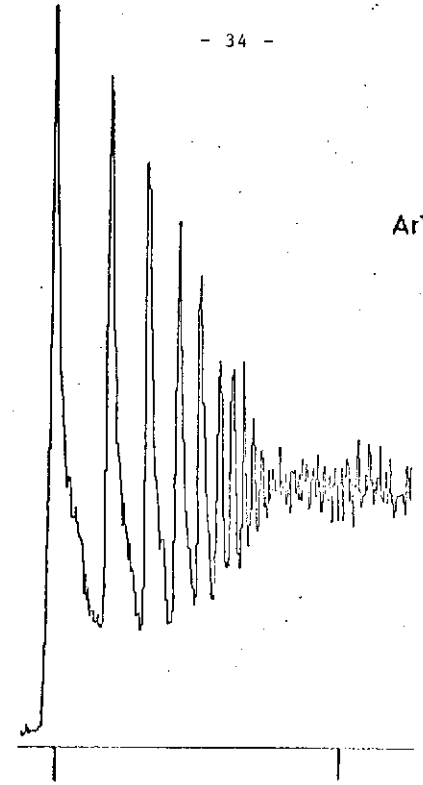

Fig. 2a)

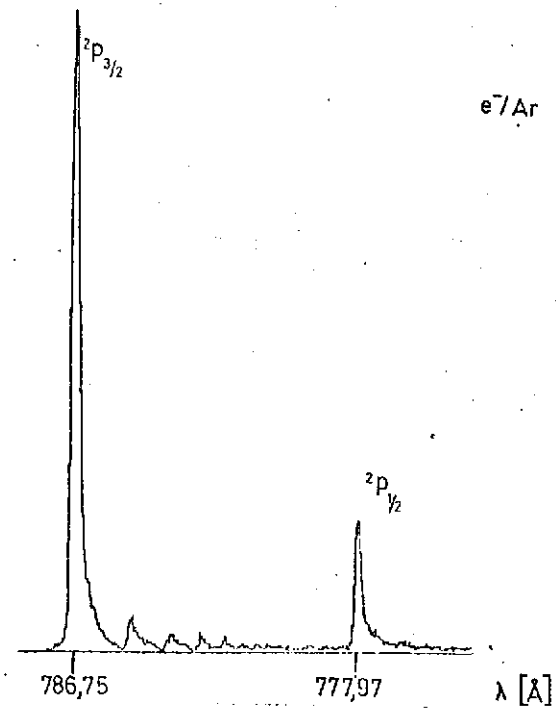

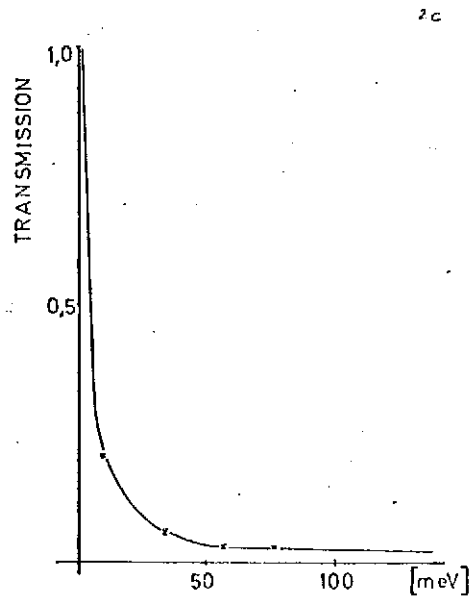
2c
TRANSMISSION
1,0
0,5
50
100
[meV]

Fig. 2c

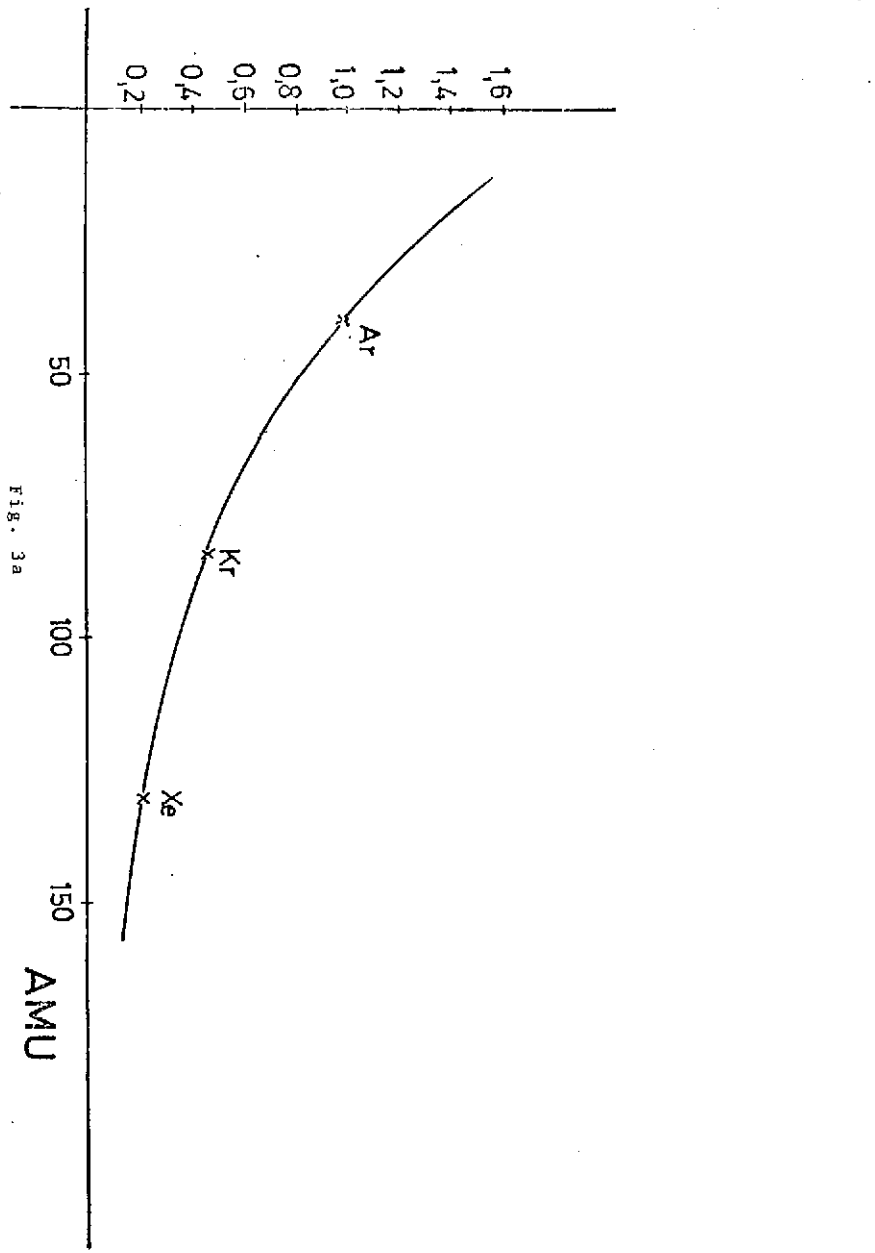
INTENSITY (ARBITRARY UNITS)
0,2
0,4
0,6
0,8
1,0
1,2
1,4
1,6
50
100
150
AMU
Ar
Kr
Xe

Fig. 3a

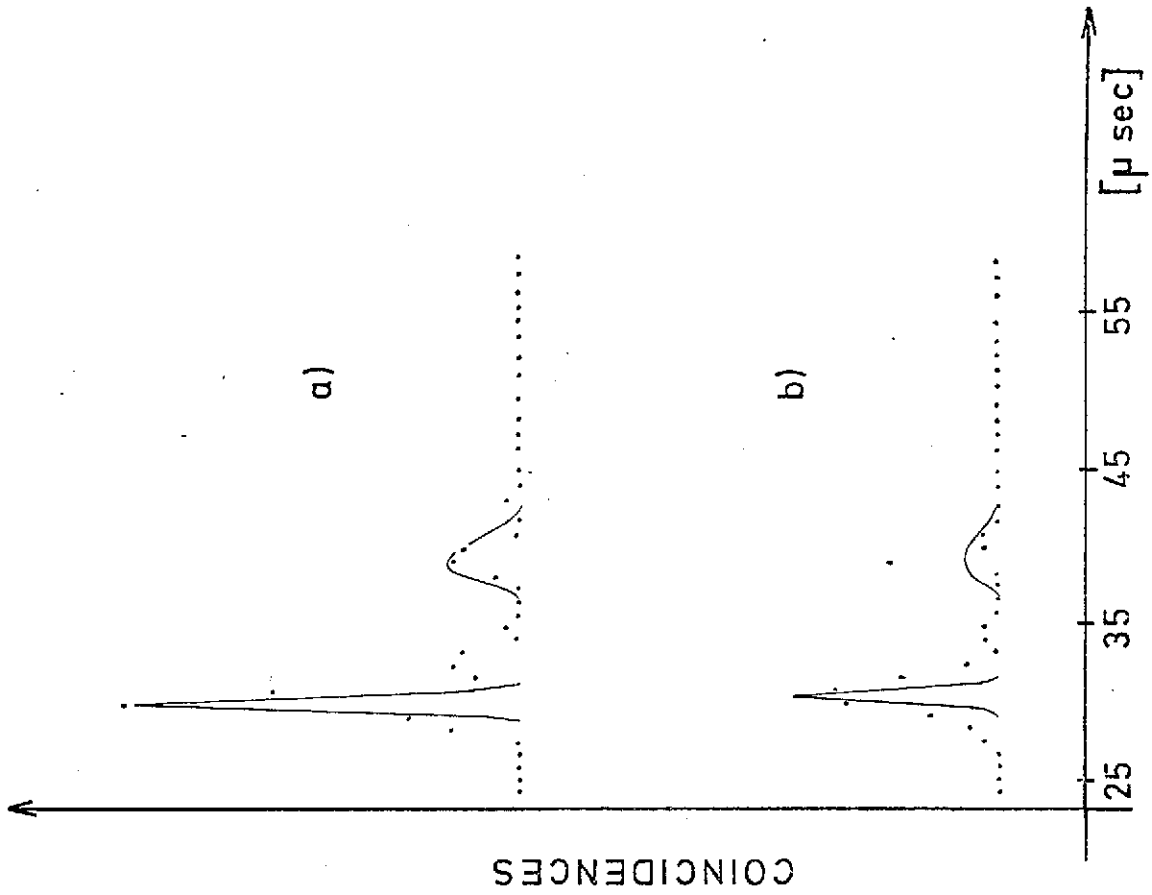
a)
b)
25
35
45
55
[μ sec]
TOF
COINCIDENCES

Fig. 4

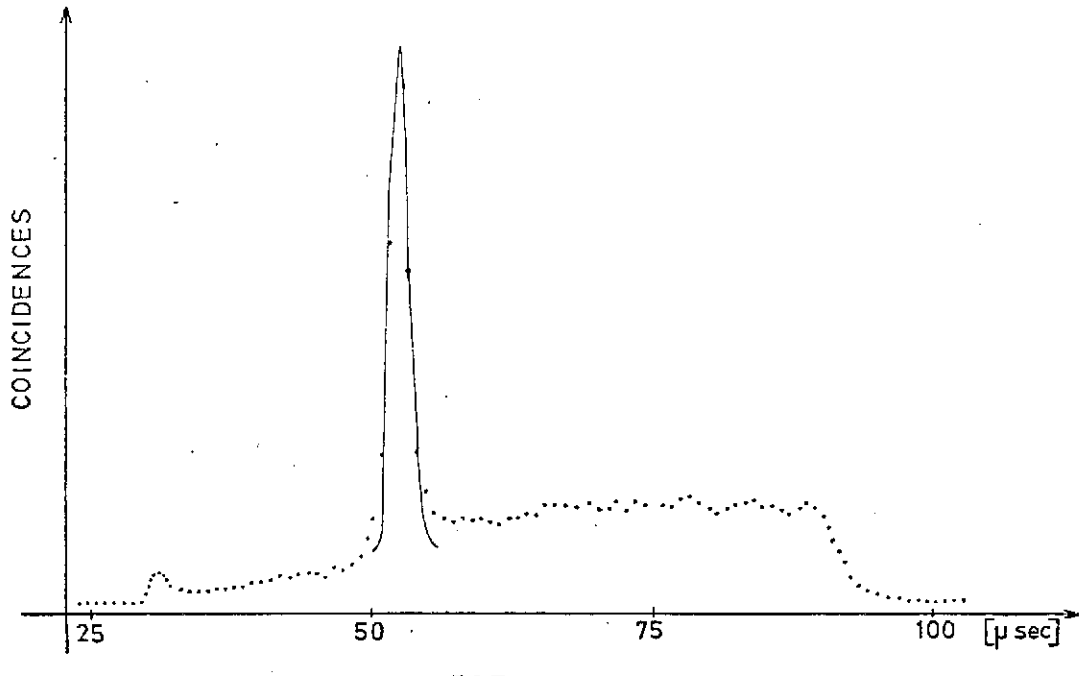
COINCIDENCES
25
50
75
100
[μ sec]
TOF

Fig. 3b

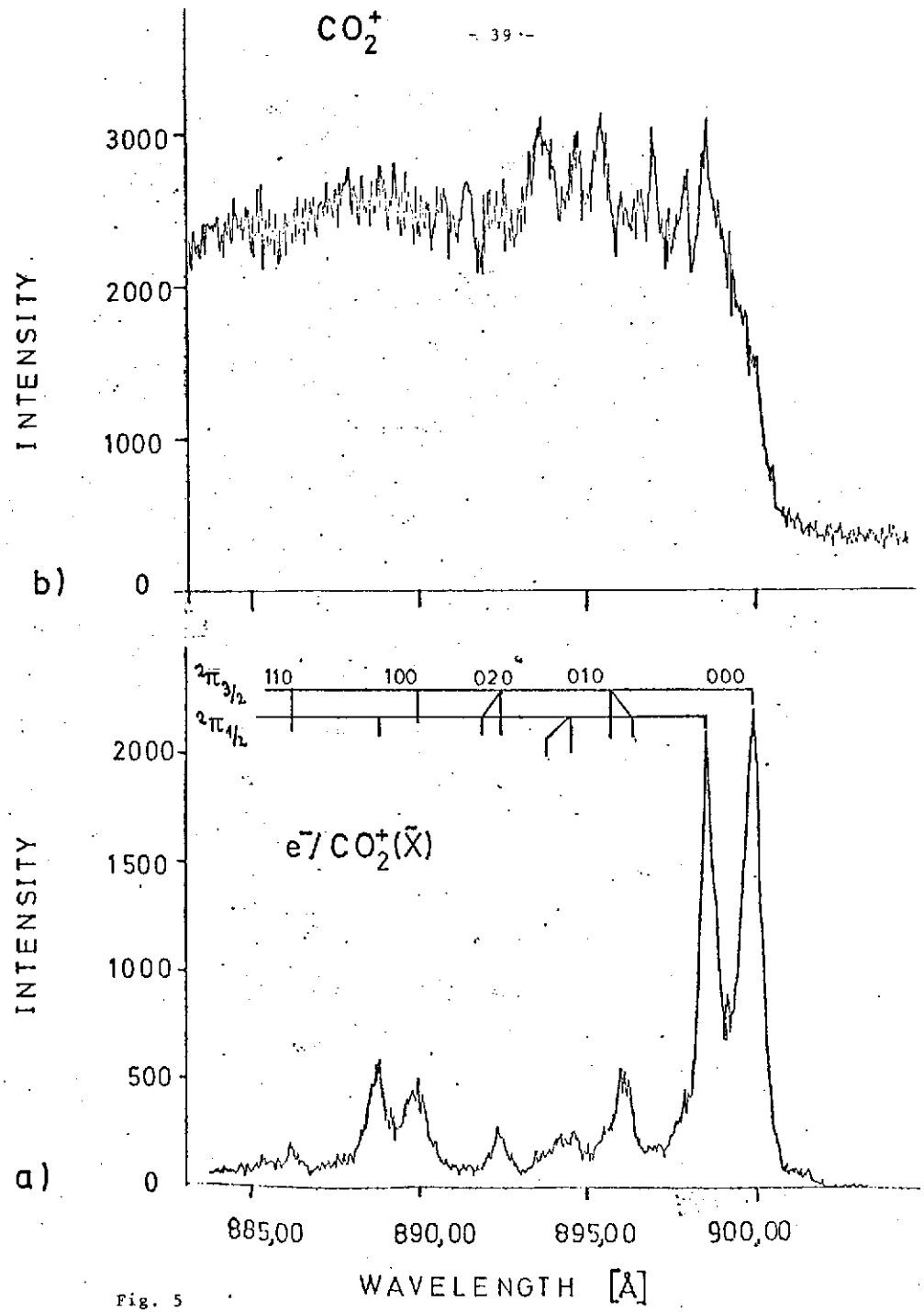
CO_2^+
INTENSITY
3000
2000
1000
0
b)
$^2\pi_{3/2}$
$^2\pi_{1/2}$
110
100
020
010
000
2000
1500
1000
500
0
$e^-/CO_2^+(\tilde{X})$
a)
885,00
890,00
895,00
900,00
WAVELENGTH [Å]

Fig. 5

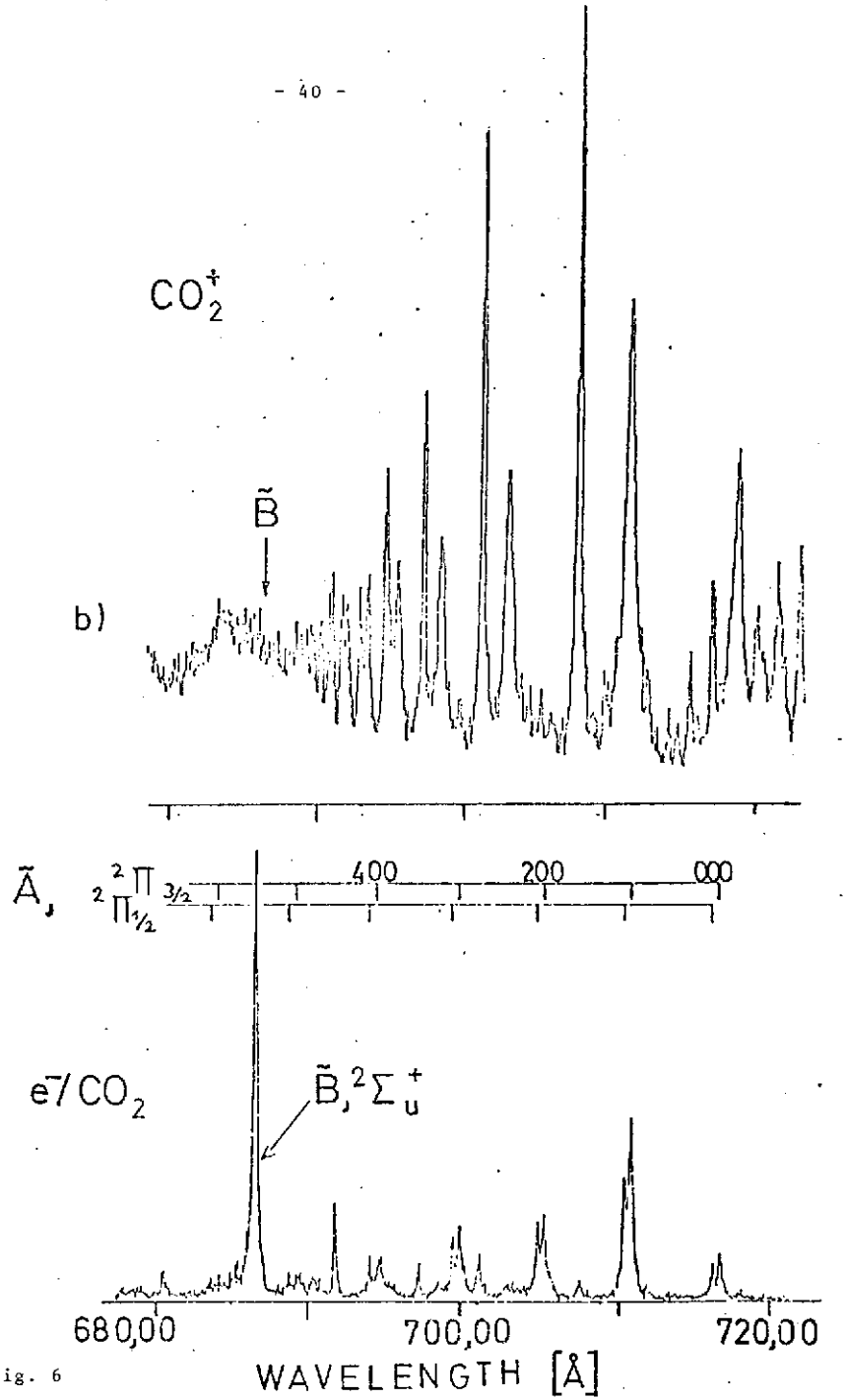
CO_2^+
$\tilde{B}$
b)
$\tilde{A}$, $^2\Pi_{3/2}$ $^2\Pi_{1/2}$
400
200
000
e^-/CO_2
$\tilde{B}, ^2\Sigma_u^+$
a)
680,00
700,00
720,00
WAVELENGTH [Å]

Fig. 6

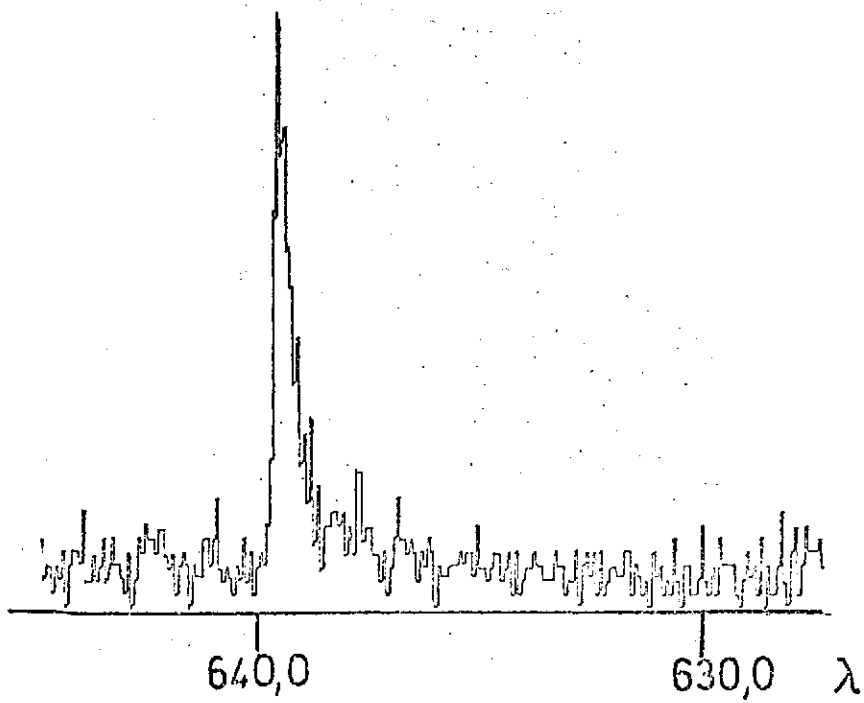

Fig. 7

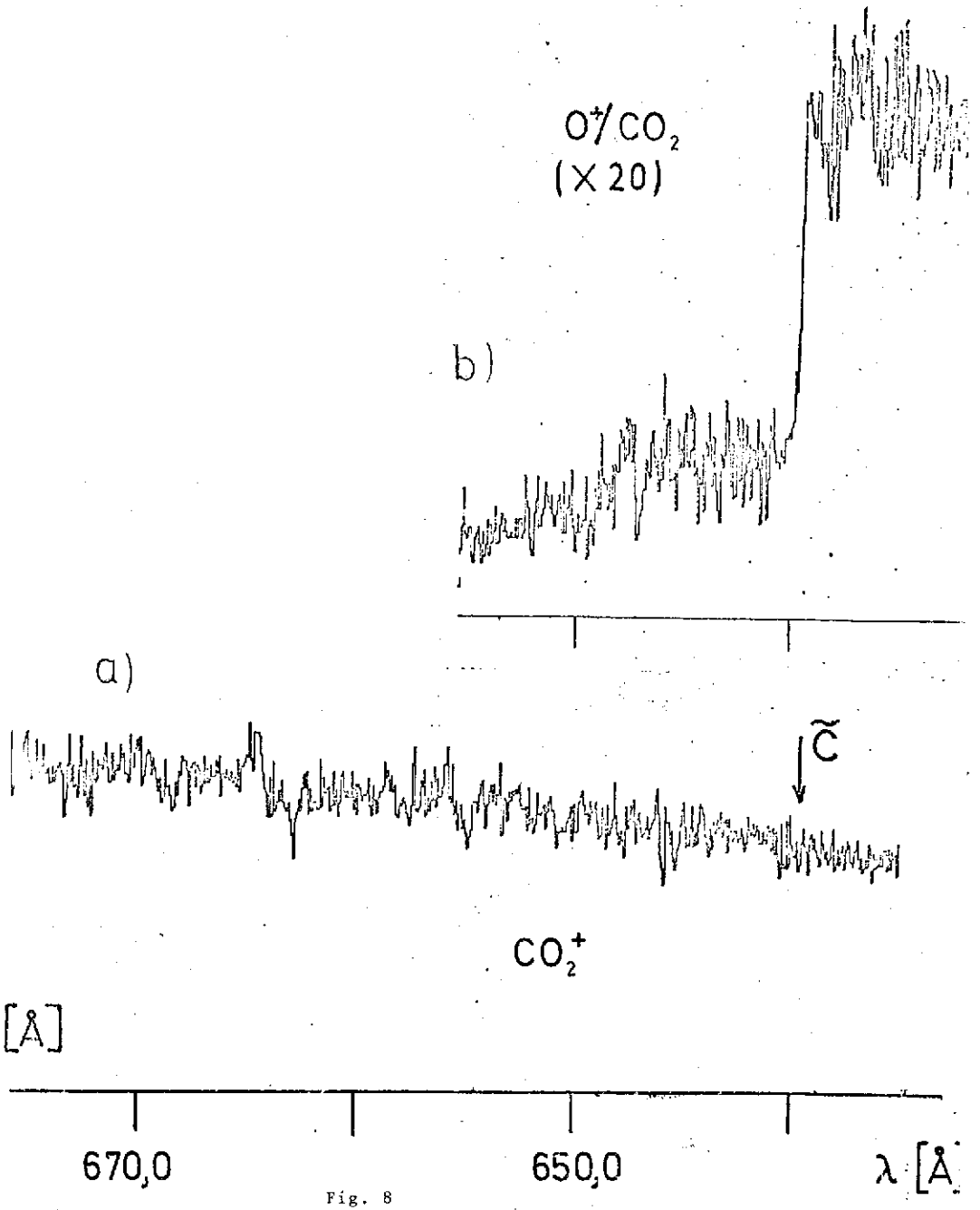

Fig. 8

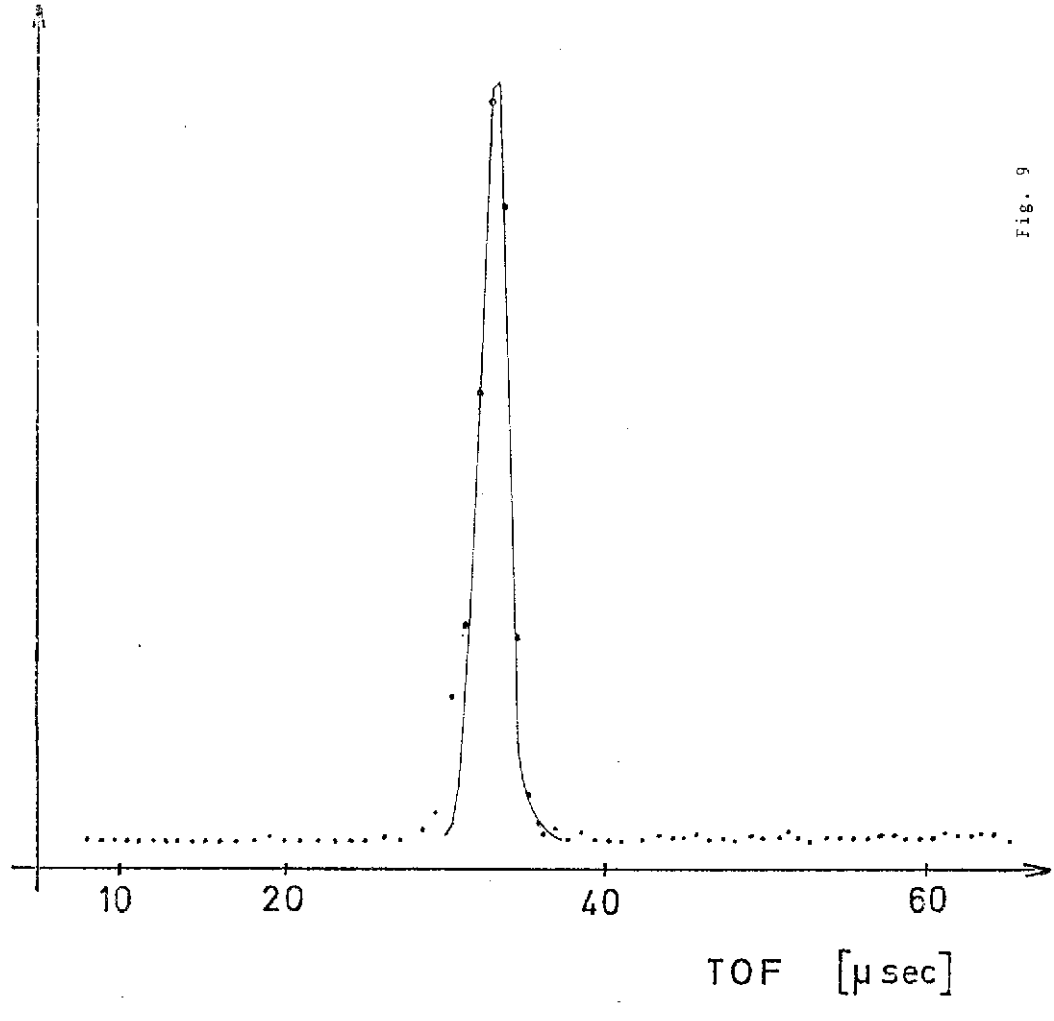

Fig. 9